Charge Selectivity of the Designed Uncharged Peptide Ion Channel Ac-(LSSLLSL)$_3$-CONH$_2$

Paul K. Kienker* and James D. Lear‡
DuPont Merck Pharmaceutical Co., Experimental Station, Wilmington, Delaware 19880 USA

ABSTRACT Charge selectivity in ion channel proteins is not fully understood. We have studied charge selectivity in a simple model system without charged groups, in which an amphiphilic helical peptide, Ac-(Leu-Ser-Ser-Leu-Leu-Ser-Leu)$_3$-CONH$_2$, forms ion channels across an uncharged phospholipid membrane. We find these channels to conduct both K^+ and Cl^-, with a permeability ratio (based on reversal potentials) that depends on the direction of the KCl concentration gradient across the membrane. The channel shows high selectivity for K^+ when [KCl] is lowered on the side of the membrane that is held at a positive potential (the putative C-terminal side), but only modest K^+ selectivity when [KCl] is lowered on the opposite side (the putative N-terminal side). Neither a simple Nernst-Planck electrodiffusion model including screening of the helix dipole potential, nor a multi-ion, state transition model allowing simultaneous cation and anion occupancy of the channel can satisfactorily fit the current-voltage curves over the full range of experimental conditions. However, the C-side/N-side dilution asymmetry in reversal potentials can be simulated with either type of model.

INTRODUCTION

The selective conduction of particular ionic species is important to the function of ion channel proteins. For instance, the excitatory nicotinic acetylcholine receptor channel is over 100-fold selective for cations (Adams et al., 1980), whereas the inhibitory $GABA_A$ and glycine receptors are over 20-fold anion-selective (Bormann et al., 1987). The difference in charge selectivity of these channels is remarkable in light of the homology among their primary amino acid sequences (Grenningloh et al., 1987; Schofield et al., 1987); this suggests that very specific features of the sequence must be involved in determining charge selectivity. Determining what these features are poses a significant challenge to ion channel biophysics.

In general, charge selectivity in ion channel proteins should depend on the pore dimensions and spatial distribution of charges. A pore of macroscopic dimensions, with a radius much greater than the Debye length, would show no more selectivity than that expected from the relative mobilities of ions in bulk solution; an ion in such a pore would interact primarily with water and other ions, rather than with the pore wall. When the Debye length is comparable with or greater than the pore radius, fixed charges in or near the pore can confer preferential charge selectivity by raising the local concentration (and, hence, electrodiffusion-driven flux) of mobile counter-ions in the pore. Representative "wide pores" (classified on the basis of sieving experiments) include the colicins (diameter $d > 9$ Å) (Raymond et al., 1985; Bullock et al., 1992), diphtheria toxin channels ($d \geq 12$ Å) (Hoch et al., 1985), and VDAC ($d \sim 30$ Å) (Blachly-Dyson et al., 1990). In addition, electron imaging of the nicotinic receptor channel shows it to have wide ($d \sim 20$ Å) "vestibules" flanking an unresolved transmembrane pore of much smaller diameter (Unwin, 1993).

At the other extreme are narrow pores, which show not only high charge selectivity, but substantial discrimination among ions of the same charge. It is thought that selectivity in narrow pores arises mainly from the balance between the energies of dehydration of an ion entering the pore and its solvation by the pore lining (Eisenman and Horn, 1983). Examples of narrow pores include voltage-gated K^+ channels ($d \approx 3$ Å), Na^+ channels ($d \approx 4$ Å), and the model channel gramicidin A ($d \approx 4$ Å) (Hille, 1992).

In between these extremes, of course, there are mid-sized pores, which show high charge selectivity, but only low selectivity among ions of the same charge. Prominent examples include the cation-selective nicotinic receptor ($d \approx 7$–8 Å) (Dwyer et al., 1980; Cohen et al., 1992b) and the anion-selective $GABA_A$ and glycine receptors ($d \approx 5$–6 Å) (Bormann et al., 1987; Fatima-Shad and Barry, 1993). In the nicotinic receptor, charged residues occupying closely similar sequence positions in homologous subunits define three "rings" of charge that have been shown to affect the single channel conductance (Imoto et al., 1988) and selectivity among cations (Konno et al., 1991). The greatest influence on this selectivity comes from the intermediate ring, together with another ring of uncharged polar residues (Villarroel and Sakmann, 1992; Cohen et al., 1992a). There is evidence that the intermediate ring mutations act through a structural change rather than by a direct electrostatic effect on the ions (Wang and Imoto, 1992). Also, the conductance changes associated with mutations in the extracellular and cytoplasmic

Received for publication 12 September 1994 and in final form 6 January 1995.

Address reprint requests to Dr. James D. Lear, Department of Biochemistry and Biophysics, University of Pennsylvania School of Medicine, Philadelphia, PA 19104-6089. Tel.: 215-898-2071; Fax: 215-898-4217; E-mail: lear@a1.mcsf.upenn.edu.

Dr. Kienker's current address: Department of Physiology and Biophysics, Albert Einstein College of Medicine, Bronx, NY 10461.

Dr. Lear's current address: Department of Biochemistry and Biophysics, University of Pennsylvania, Philadelphia, PA 19104-6089.

0006-3495/95/04/1347/12 $2.00

rings show a weaker ionic strength dependence than would be expected from double-layer theory (Kienker et al., 1994b).

The sign of the net "ring" charge of the homologous acetylcholine- and $GABA_A$-receptor channel proteins has been pointed out to correlate with their selectivity to ions of opposite charge (Green and Andersen, 1991). However, reports of directed mutations affecting charge selectivity in mid-sized protein channels are surprisingly rare, given the number of mutations that have been made. Particularly informative is a recent report (Galzi et al., 1992) of a series of mutations directed toward transforming the "M2" segment of the cation-selective neuronal nicotinic acetylcholine receptor channel into segments resembling those of the anion-selective $GABA_A$-receptor channel. Changing the negatively charged "intermediate ring" residues of the nicotinic receptor segment to neutral ones did not alone change the charge selectivity of the channel; insertion of an additional, uncharged residue into the mutant sequence was necessary to make the channels anion-selective. Although it has been suggested that the inserted residue produces a structural change that moves a positively charged residue nearer to the pore (Imoto, 1993), more subtle mechanisms could be involved, such as reducing the pore diameter or changing side chain orientations. Moreover, studies of model peptide ion channels also indicate that fixed charges in general do not determine charge selectivity. For example, the gramicidin A channel has no charged groups and is highly cation-selective (Myers and Haydon, 1972). Analogs of alamethicin with negative, positive, or no charge all form weakly cation-selective channels (Hall et al., 1984), as do a number of peptides containing basic residues, but no acidic groups (Sansom, 1991; Åkerfeldt et al., 1995). One study of peptide ion channels modeled after the glycine receptor indicated that fixed charges confer charge selectivity (Reddy et al., 1993), but a similar study found that a given peptide can form channels with a variety of selectivities (Langosch et al., 1991). It appears, then, that the complete molecular mechanism of charge selectivity in mid-sized pores is not yet understood (Sather et al., 1994), and it would be desirable to have a simple model system to study charge selectivity in a systematic way.

Previously, we studied such a system: a 21-residue amphiphilic α-helical channel-forming peptide, H_2N-(Leu-Ser-Ser-Leu-Leu-Ser-Leu)$_3$-$CONH_2$. Single-channel conductance measurements indicated about a 10-fold cation selectivity, with little discrimination among small monovalent cations and measurable single-channel conductance to cations as large as $Tris^+$, but not to glucosammonium, indicating a "mid-sized" pore of about 8-Å diameter (Lear et al., 1988). We wished to determine charge selectivity more quantitatively from reversal potentials, but the strong voltage dependence of channel formation and the short open channel lifetimes made this appear to be too difficult a task. We found, however, that the N-acetylated analog Ac-(Leu-Ser-Ser-Leu-Leu-Ser-Leu)$_3$-$CONH_2$ (Ac-(LSSLLSL)$_3$) has longer channel lifetimes (Åkerfeldt et al., 1993; Kienker et al., 1994a), making it practical to measure complete single-channel current-voltage relations and reversal potentials by using fast voltage pulses and ramps. Because this peptide is uncharged, it also provides an ideal model system to investigate how uncharged groups can contribute to charge selectivity in mid-sized protein channels. Here, we report detailed, quantitative measurements of the charge selectivity of the Ac-(LSSLLSL)$_3$ channel, and present two elementary theoretical treatments of the data that attempt to relate our observations to our structural model for this channel. This work has been presented in a preliminary form (Kienker et al., 1993).

MATERIALS AND METHODS

Bilayer experiments

The peptide Ac-(LSSLLSL)$_3$ was synthesized and purified as described previously (Kienker et al., 1994a). Planar bilayer membranes were formed in a 50- to 80-μm hole (created by electrical discharge) in a Teflon film, pretreated with 10 nl of squalane in pentane. The film separated a pair of 2-ml chambers in a Teflon block. The chambers were cleaned with water and methanol and stored in chromic/sulfuric acid; they were rinsed thoroughly with water before use. Diphytanoylphosphatidylcholine lipid (Avanti Polar Lipids, Alabaster, AL) in pentane was added to the bath solutions, and bilayer membranes were formed by monolayer apposition (Montal and Mueller, 1972). Squalane, pentane, and lipid were purified as described (Kienker et al., 1994a). The membrane potential was held at −200 mV for 30 min to confirm bilayer stability before peptide addition. About 300 pmol of peptide (150:1 lipid/peptide dissolved in methanol) was added to each bath solution, and the membrane was broken and reformed repeatedly to incorporate peptide. If necessary during the course of the experiment, more peptide or lipid was added and the membrane was reformed. Open channel properties were similar with peptide added to only one bath. Also, the open probability showed a voltage sensitivity similar to that reported previously (Lear et al., 1988; Åkerfeldt et al., 1993) for the nonacetylated peptide.

Because some channels are known to exhibit a pH-dependent charge selectivity (Raymond et al., 1985), we tested both neutral and low pH solutions. The pH 7 bath solutions contained the specified salt and 5 mM HEPES, 0.2 mM EDTA, and KOH (or triethanolamine) to pH 7.0. The pH 3 solutions contained the specified salt and HCl to pH 3.0. KCl and K_2SO_4 (J. T. Baker, Phillipsburg, NJ) were roasted overnight at 550°C before use. K glucuronate was prepared from D-glucuronic acid (Aldrich Chemical Co., Milwaukee, WI) and KOH (EM Science, Gibbstown, NJ) by crystallizing from aqueous solution and washing with cold water and diethyl ether; product identity was confirmed by mass spectrometry. The triethanolammonium glucuronate solution was prepared from triethanolamine (Eastman Kodak, Rochester, NY), and D-glucuronic acid (Fluka, Ronkonkoma, NY). D-glucosamine HCl (Kodak), K glucuronate, and triethanolammonium glucuronate solutions were purified by pentane extraction. Bath solutions were changed by withdrawing a sample and replacing with an equal volume of a new solution.

Ag/AgCl electrodes were prepared by electroplating in 1 M HCl and were placed in reservoirs containing the 1 M KCl bath solution, with 1% agarose salt bridges leading to the bath chambers. Single-channel currents were recorded with an EPC-7 amplifier (List/Medical Systems, Greenvale, NY), an 8-pole lowpass Bessel filter (Frequency Devices, Haverhill, MA), a Labmaster D/A converter, TL-1 interface, AI2020A event detector, and pCLAMP software (Axon Instruments, Foster City, CA), modified as described (Kienker et al., 1994a). Current-voltage data were obtained primarily by 20-ms voltage ramps from the holding potential to the opposite potential, triggered during an open channel event by the event detector, using 2-kHz filtering and 10-kHz sampling. The holding potential was maintained continuously between ramps, for better baseline subtraction. At the end of an experiment, the bath solutions were restored to the initial concentration before measuring the electrode offset potential. All experiments were conducted at room temperature, 22–23°C.

Data analysis

Bath solution concentrations were determined by measuring the conductivities of the withdrawn samples and standard solutions with a CDM80 conductivity meter (Radiometer, Copenhagen). Activity coefficients for KCl and K_2SO_4 were taken from tables (Parsons, 1959; Robinson and Stokes, 1968). K glucuronate and glucosammonium Cl activity coefficients were estimated by measuring osmolalities (at 37°C) with a model 5500 vapor pressure osmometer (Wescor, Logan, UT). The osmotic coefficient ϕ was fit as a function of molal concentration m using the formula (Robinson and Stokes, 1968)

$$\phi = 1 - \alpha m^{0.5}\sigma(\beta m^{0.5}) / 3 + bm, \quad (1a)$$

with

$$\sigma(x) = (3/x^3)[(1 + x) - 2\ln(1 + x) - (1 + x)^{-1}] \quad (1b)$$

which by the Gibbs-Duhem equation gives the activity coefficient γ as

$$\gamma = \exp[-\alpha m^{0.5}/(1 + \beta m^{0.5}) + 2bm]. \quad (2)$$

For K glucuronate we used the parameter values $\alpha = 7.53$, $\beta = 5.53$, and $b = -0.116$; for glucosammonium Cl, we used $\alpha = 4.99$, $\beta = 2.79$, and $b = 0.0651$. Single-ion activity coefficients were assumed to equal the mean salt activity coefficient. Liquid junction potentials were calculated from the Henderson equation (Ammann, 1986), using bulk mobilities u from tables (Robinson and Stokes, 1968) or estimated from conductivity measurements ($u_{\text{glucuronate}}/u_K \approx 0.333$, $u_{\text{triethanolammonium}}/u_K \approx 0.483$).

Currents were analyzed using our modified pCLAMP software. Single-channel currents were obtained by subtracting baseline ramp currents (with no channel events) from the total membrane current. Only events with good baseline subtraction were analyzed further. Most Ac-(LSSLLSL)$_3$ channels (at a 200-mV holding potential with 1 M KCl, pH 7) had a chord conductance between 120 and 230 pS; however, we have observed channels with conductances as large as 640 pS and as small as 5 pS (Fig. 1). We do not know the source of this heterogeneity of conductances. To control for this heterogeneity, we restrict our analysis to channels in the most common conductance range (155 ± 10 pS under these conditions). We have not attempted macroscopic (many-channel) selectivity measurements, because a different conductance state might predominate under those conditions. A histogram of holding currents was constructed to limit the analyzed channel population to those within approximately ±10% of the most frequently observed pre-pulse channel current under each solution condition. Each single-channel current-voltage relation presented is an average of typically 20–70 individual ramps; only ramps with a well resolved current reversal were used. An exception was made to this rule when the reversed current was too small for reliable identification; in this case only channels that stayed open beyond the end of the first ramp, and into the return ramp, were analyzed (Fig. 2). Reversal potentials were estimated by fitting a fifth-order polynomial to the averaged current-voltage relation for further noise reduction. Individual single-channel ramp currents were too noisy for reversal potential determination. Theoretical models were fit using the programs KaleidaGraph (Synergy Software, Reading, PA) and MLAB (Civilized Software, Bethesda, MD).

The orientation of channels formed by the peptide Ac-(LSSLLSL)$_3$ depends on the polarity of the holding potential. Because we did experiments using both positive and negative holding potentials, referred to the virtual ground of the amplifier, to avoid confusion we adopted the sign convention that the holding potential is always negative (except in Figs. 1 and 2, which present "raw" data). Because of the similarity in conductance and voltage-dependent gating properties to the previously studied, nonacetylated analog, we maintained the same working model for the channel structure: an aggregate of parallel α-helices, with the peptide helix dipoles aligned with the transmembrane electric field. In this model, the N termini would be on the side of the membrane, which is held at a negative potential, and the C termini would be on the opposite side. Correspondingly, any subsequently changed membrane potential would be defined as the potential on the "N side" relative to the "C side" (Fig. 3).

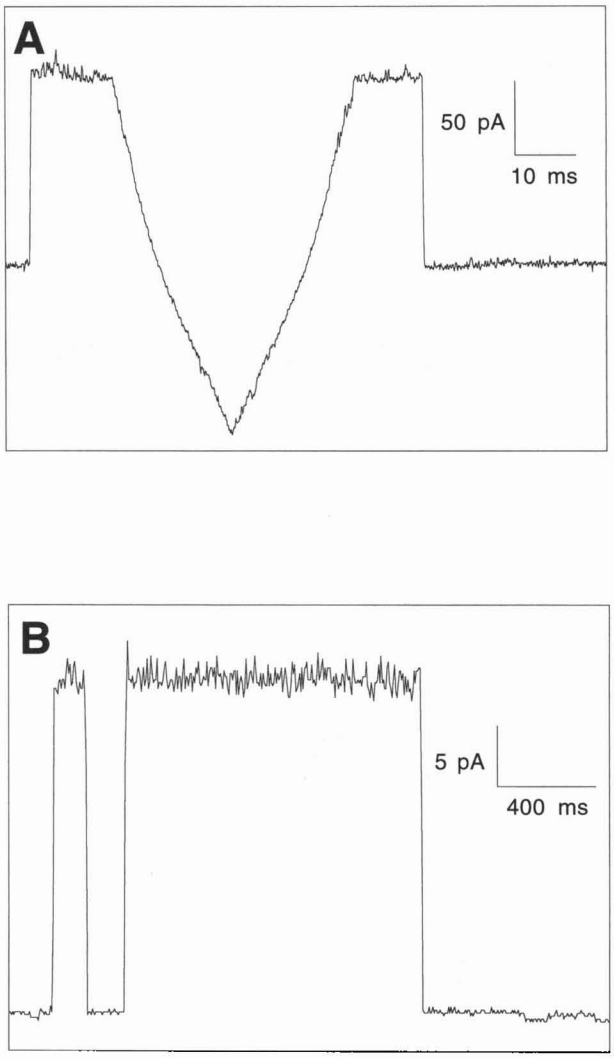

FIGURE 1 A sample of the different sizes of Ac-(LSSLLSL)$_3$ single-channel currents in 1 M KCl, pH 7. (*A*) Large channel, 128 pA at the holding potential of 200 mV. The curved "V"-shaped current deflection in the middle of the channel event was caused by a linear voltage ramp to −200 mV and back to 200 mV. There is also a "normal-sized" channel open throughout the trace. $f = 2$ kHz. (*B*) "Normal" and small channels, 28 and 1 pA at 200 mV. $f = 100$ Hz.

RESULTS

Currents in symmetric KCl solutions

We first measured the dependence of the Ac-(LSSLLSL)$_3$ single-channel conductance on salt concentration in symmetric solutions of KCl, pH 7. The current-voltage relations show greater rectification at lower KCl concentration (Fig.4). The shape of the conductance-activity relation depends on the membrane potential, with a linear dependence at zero and positive voltages, and a weakly sublinear dependence at negative voltages (Fig. 5).

Selectivity under [KCl] gradients

We next measured the charge selectivity of Ac-(LSSLLSL)$_3$ channels in asymmetric solutions of KCl, pH 7. We began

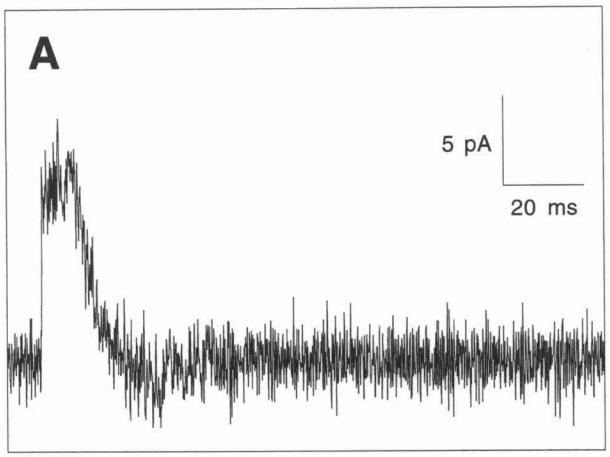

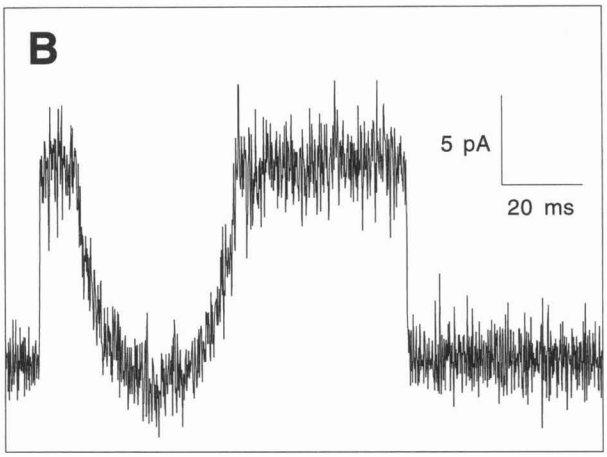

FIGURE 2 Use of voltage ramps to obtain current-voltage data from single Ac-(LSSLLSL)$_3$ channels in KCl, pH 7. (*A*) When the current at the "reversed" voltage is small, it can be difficult to determine precisely when the open channel current ends. (*B*) When a channel remains open through the first ramp and into the return ramp, it is clear that the entire ramp represents open channel current. Ramps from 170 to −170 mV and back. [KCl] = 1.1 M on the side of the membrane held at a positive potential and 0.062 M on the opposite side. f = 2 kHz.

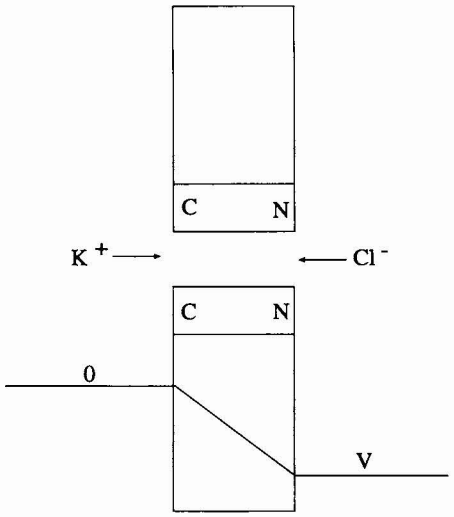

FIGURE 3 Hypothesized orientation of Ac-(LSSLLSL)$_3$ channels with respect to the holding potential. By our convention, following this model, the side of the membrane held at a negative potential is called the "N side," and the opposite side is called the "C side."

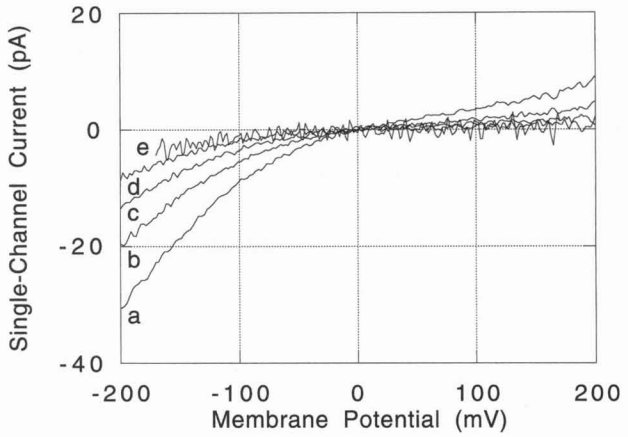

FIGURE 4 Averaged Ac-(LSSLLSL)$_3$ single-channel current-voltage data in symmetric KCl, pH 7. [KCl] (M) C-side/N-side: (curve a) 1.0/1.0; (curve b) 0.50/0.50; (curve c) 0.25/0.24; (curve d) 0.12/0.12; (curve e) 0.071/0.068.

each of these experiments in symmetric 1 M KCl, and diluted on either the C side or the N side, as defined above. With dilution on the C side, the negative branch of the single-channel current-voltage curve decreased in amplitude, whereas the positive branch did not change much, indicating high selectivity for K^+ over Cl^- (Fig. 6 *A*). The reversal potential shifted to a negative voltage, by 42 ± 1 mV for a 10-fold salt activity gradient (Fig. 7); fitting these C-side dilution data with the Goldman-Hodgkin-Katz formula (Hille, 1992) gives a permeability ratio $P_K/P_{Cl} = 16$. Dilution on the N side is not the mirror image of C-side dilution. With N-side dilution, the current decreased at both positive and negative voltages, with a proportionately greater decrease at positive voltages (Fig. 6 *B*). The reversal potential shifted to positive voltage, by 18 ± 1 mV for a 10-fold gradient (Fig. 7), indicating relatively weak selectivity for K^+ over Cl^- ($P_K/P_{Cl} = 2.4$). The data from both sides can be fit by allowing the permeability ratio to depend on the C-side/N-side KCl activity ratio R, with the empirical formula $P_K/P_{Cl} = 5.2\ R^{-0.35}$ (Fig. 7). Thus, the Ac-(LSSLLSL)$_3$ channel selectivity, as conventionally defined by measured reversal potentials, has an asymmetric dependence on the KCl activity gradient.

K:Cl selectivity at low pH

We also examined Ac-(LSSLLSL)$_3$ selectivity in 1 M KCl, pH 3. The selectivity appears qualitatively the same as at pH 7, with greater K^+ selectivity for C-side dilutions than for N-side dilutions. Overall, the channel is slightly less K^+-selective at pH 3 than at pH 7, and even appears weakly

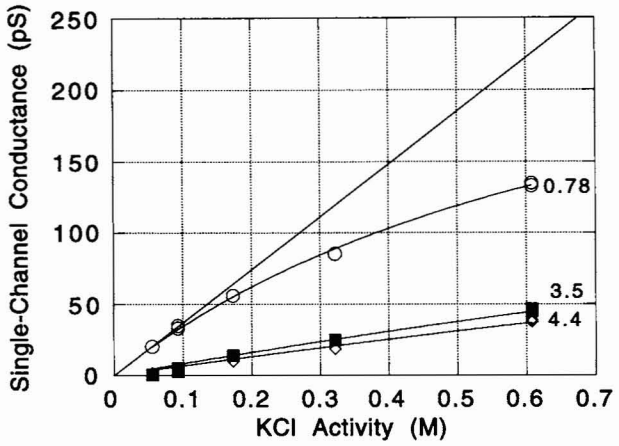

FIGURE 5 Ac-(LSSLLSL)$_3$ single-channel conductance-activity relations at different membrane potentials, from polynomial fits of Fig. 4 data. (○) −170 mV; (■) 0 mV; (◇) 170 mV. Data at 0 mV are slope conductances; others are chord conductances. The straight line, with slope 370 pS/M, is drawn to emphasize the sublinearity of the −170 mV curve. The curves are fit by the Michaelis-Menten formula $g = g_{max}/(1 + K_m/a_{KCl})$, using g_{max} = 304 pS for all curves, and K_m (in M) as indicated on the graph.

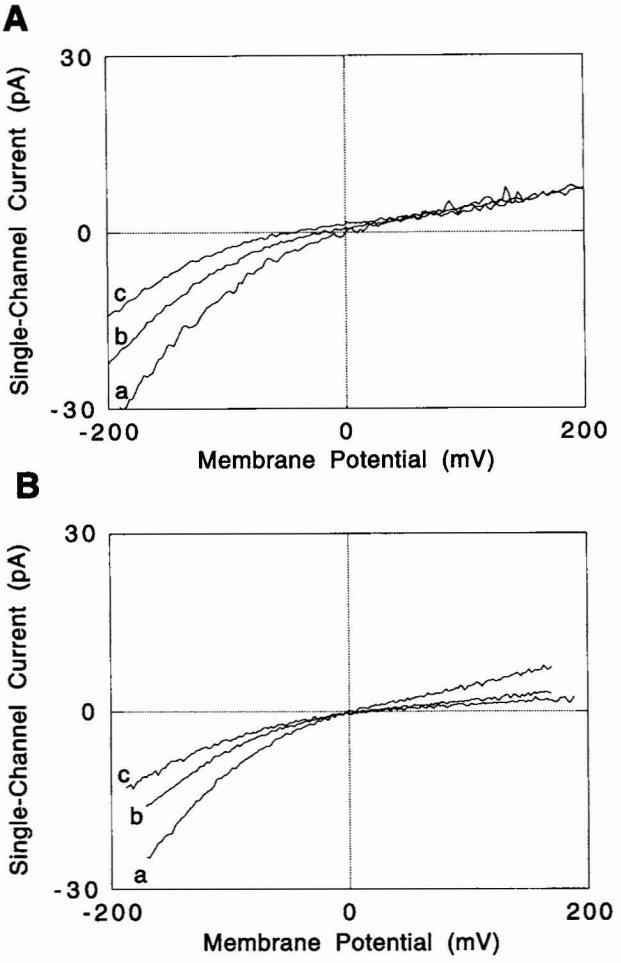

FIGURE 6 Averaged Ac-(LSSLLSL)$_3$ single-channel current-voltage data in asymmetric KCl solutions, pH 7. (*A*) C-side dilutions. [KCl] (M) C-side/N-side: (curve a) 1.0/1.0; (curve b) 0.24/1.0; (curve c) 0.053/1.1. (*B*) N-side dilutions. [KCl] (M) C-side/N-side: (curve a) 1.0/1.0; (curve b) 1.0/0.24; (curve c) 1.1/0.069.

Cl^--selective for large N-side dilutions (Fig. 7). The Goldman-Hodgkin-Katz theory cannot fit the N-side dilution branch of this curve using a single permeability ratio; fitting as above gives the formula $P_K/P_{Cl} = 4.2\ R^{-0.76}$. The difference from pH 7 is most likely due to a positive surface charge on the phosphatidylcholine membrane at pH 3; it has been shown that phosphatidylethanolamine membranes are partially charged at this pH (McLaughlin et al., 1970). We note that the resistance of our unmodified bilayer membranes (before peptide addition) also depends on pH, being highly resistive at pH 3 (>100 GΩ), but less so at pH 7 (typically 20 GΩ at 200 mV in 1 M KCl); we do not know the cause. In any case, we observe an even greater dependence of reversal potential on the dilution side at pH 3 than at pH 7.

Permeability of large ions

We wished to identify impermeant ions to estimate the pore diameter, and also to control ionic strength and osmotic effects. We measured single-channel currents and determined reversal potentials for salt gradients of either 0.5 M K glucuronate, pH 7, or 0.5 M K_2SO_4, pH 3 (Fig. 7). The reversal potential corresponding to a 10-fold activity ratio was 57 ± 1 mV for K glucuronate N-side dilution and 62 ± 4 mV for K_2SO_4 with either N-side or C-side dilution, which is consistent with the impermeance of the glucuronate and sulfate anions. Based on our results in KCl, the N-side dilutions are expected to give the most sensitive test of anion impermeance. These experiments also indicate that osmotic effects on permeation are small under these conditions, as streaming potentials resulting from the water activity gradients would reduce the magnitude of the reversal potentials.

We also examined the permeability of glucosammonium, as a cation counterpart to the impermeant glucuronate anion. To identify the conductance state corresponding to the predominant state in K^+ solutions, we monitored the decrease in single-channel conductance as KCl was progressively replaced on both sides of the membrane with glucosammonium Cl, both at 1 M concentration, pH 3. With the high holding potentials we used here, we readily observed small single-channel currents in pure glucosammonium Cl (Fig. 8). If glucosammonium is impermeant, as expected by analogy with glucuronate, then these currents (~3 pA) must be carried by Cl^-. (Proton currents should be ~0.3 pA, based on the aqueous mobility of H^+ relative to K^+.) We were not able to determine glucosammonium permeability directly in a salt-gradient experiment, because the reversal potentials could not be measured reliably for these low conductance channels. (It is likely that the same difficulty would be encountered for any weakly permeant cation with Cl^- as a counterion.) However, using the permeability ratio P_K/P_{Cl} estimated from Fig. 7 (4.2 for symmetric 1 M KCl, pH 3), and accounting for the twofold difference in KCl and glucosammonium Cl activity coefficients leads to the prediction $g_{KCl}/g_{Cl} \approx 9$. The fact that this is close to the observed $g_{KCl}/$

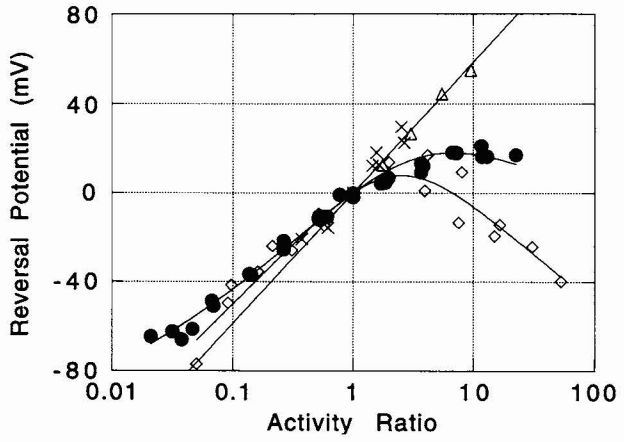

FIGURE 7 Ac-(LSSLLSL)$_3$ reversal potentials plotted against C-side/N-side salt activity ratio R. $R < 1$, C-side dilutions; $R > 1$, N-side dilutions. (●) KCl, pH 7. Fit curve uses the Goldman-Hodgkin-Katz formula, allowing the K^+/Cl^- permeability ratio to depend on the KCl activity ratio according to the empirical formula $P_K/P_{Cl} = 5.2\ R^{-0.35}$. (◇) KCl, pH 3. Fit curve as above, with $P_K/P_{Cl} = 4.2\ R^{-0.76}$. (△) K glucuronate, pH 7. (X) K_2SO_4, pH 3. The straight line indicates the K^+ equilibrium potential, which is the expected reversal potential if the anion is impermeant. The salt concentration on the undiluted side is 1 M (KCl experiments) or 0.5 M (others).

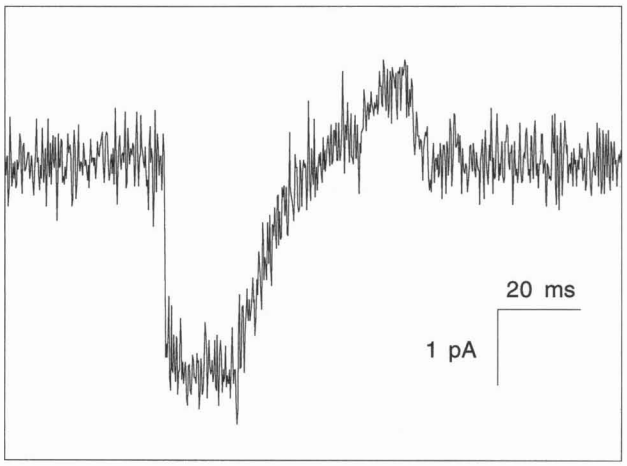

FIGURE 8 Ac-(LSSLLSL)$_3$ single-channel current in 1 M glucosammonium Cl, pH 3, during a voltage ramp from a −200 mV holding potential to 200 mV. The channel closed near the time that the return ramp began. f = 1 kHz.

$g_{glucosammoniumCl} \approx 10$ suggests that glucosammonium is impermeant. We also note that our previously proposed model for current rectification in Ac-(LSSLLSL)$_3$ channels (Kienker et al., 1994a) predicts that K^+ and Cl^- currents should rectify in the same direction; thus, it is not surprising that we observe "N-ward" rectification both in KCl (in which K^+ conduction predominates) and in glucosammonium Cl (in which we suspect that Cl^- conduction predominates). Thus, although not conclusive, our data are consistent with glucosammonium being impermeant.

The previous experiments show that glucuronate is impermeant and suggest that the similarly large glucosammonium is also impermeant. An obvious next step would be to use glucosammonium glucuronate as an impermeant salt to control ionic strength and osmotic effects; unfortunately, we were unable to prepare this salt because of the extreme oxidation sensitivity of free glucosamine. Based on studies of nicotinic receptor permeability (Dwyer et al., 1980), we selected triethanolammonium as another candidate impermeant cation. We then repeated the 1 M KCl, pH 7, N-side dilution experiment, but instead of substituting KCl-free buffer solution for the 1 M KCl electrolyte, we used 1 M triethanolammonium glucuronate, pH 7 to maintain an approximately constant ionic strength. The resulting current-voltage relations are quite close to those from the original protocol (Fig. 9), although the small decrease seen in the reversal potentials could indicate a slight permeability to triethanolammonium. The similarity of the current-voltage relations suggests that changes in ionic strength with dilution of the bathing solutions are not primarily responsible for the apparent changes in selectivity.

DISCUSSION

This study of the charge selectivity of Ac-(LSSLLSL)$_3$ channels was undertaken in the hope of gaining insight into the origins of charge selectivity in mid-sized protein ion channels. We find that Ac-(LSSLLSL)$_3$ channels show permeability to both K^+ and Cl^- but also, under some conditions, show a significant degree of selectivity between these ions. The determinants of charge selectivity in this channel are unstable; reversing the direction of an approximately 10-fold salt concentration gradient across the membrane can produce a sevenfold change in apparent charge selectivity. The trend in the permeability ratio (P_K/P_{Cl}) depends on the presumed orientation of the peptide, showing high cation selectivity for C-side dilutions, but only weak cation selectivity for N-side dilutions.

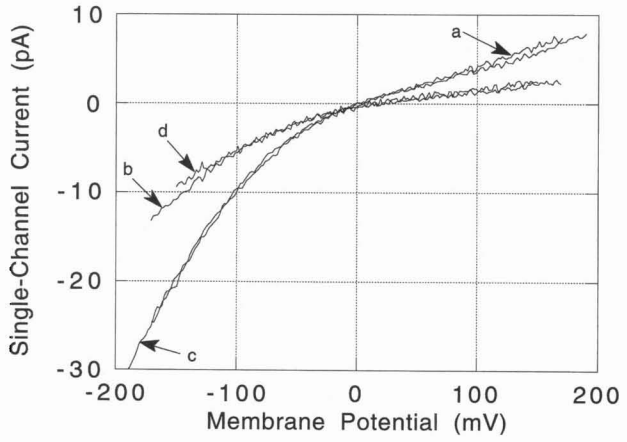

FIGURE 9 Attempt to control ionic strength. Averaged Ac-(LSSLLSL)$_3$ single-channel current-voltage data in KCl, pH 7. (curves a and b) N-side replacement of 1 M KCl with KCl-free pH 7 buffer, as in Fig. 6 *B*; (curves c and d) N-side replacement with 1 M triethanolammonium glucuronate, pH 7. [KCl] (M) C-side/N-side: (curve a) 1.0/1.0; (curve b) 1.0/0.11; (curve c) 0.98/0.98; (curve d) 1.0/0.12.

The Ac-(LSSLLSL)$_3$ channel has characteristics of both mid-sized and wide pores. Ion-sieving experiments indicate that its pore diameter is close to that of the nicotinic receptor. However, unlike the nicotinic receptor, which is more than 100-fold cation-selective, the selectivity of Ac-(LSSLLSL)$_3$ channels between K^+ and Cl^- is more characteristic of a wide pore, with a modest level of cation selectivity that is subject to experimental modulation. This sensitivity to experimental conditions is encouraging, we think, in that subsequent "design" changes in this elementary sequence have at least the potential to provide more extreme levels of both cation and anion selectivity.

To help understand these results more quantitatively, as well as to help guide future design efforts, we have considered two factors that could contribute to the asymmetric charge selectivity that we have observed in Ac-(LSSLLSL)$_3$ channels: the dipole potential of parallel peptide helices forming the channel, and interactions between cations and anions within the channel. In the following sections, these factors are examined in the context of simplified mathematical models appropriate for examining specific effects: an electrodiffusion model for the electrical dipole effects, and a multi-ion occupancy, state transition model for treating ion-ion channel interactions.

Electrodiffusion model

The dipole moments of the peptide bonds in an α-helix are oriented nearly parallel to the helix axis, giving rise to a molecular macrodipole (Wada, 1976). The helix dipole potential contributes to the energetics of protein folding and catalysis (Hol, 1985) and is subject to electrolyte screening (Lockhart and Kim, 1993). The dipole potential of parallel helical peptides lining an ion channel should concentrate cations at the C terminus and anions at the N terminus. Insofar as ion entry into the channel is the rate-limiting step in conduction (a supposition supported by the nearly linear conductance-activity relations in Fig. 5), these local concentration changes could affect the charge selectivity of the channel. Lowering the ionic strength (bulk salt concentration) on the N side could increase the positive potential of the N terminus, thereby favoring anion conduction; C-side ionic strength reduction likewise could favor cation conduction, a possible qualitative explanation for the result we observe.

We explored this helix dipole model more quantitatively, using an extension of the Nernst-Planck electrodiffusion model described previously (Kienker et al., 1994a), but allowing for the independent fluxes of K^+ and Cl^-, with a permeability ratio $P_\pm$ reflecting intrinsic selectivity that is not due to the helix dipole potential. As before, the helix dipole potential was approximated as the potential produced by a partial positive charge at the N terminus of each peptide, and an opposite partial charge at the C terminus. The magnitude of this charge was a parameter of the model. To account for electrolyte screening in a simple way, the end-charge magnitude was multiplied by $\exp(-\kappa r)$, where r is the pore radius (4 Å) and $1/\kappa$ is the Debye length in the adjacent bulk solution.

We fit this electrodiffusion model simultaneously to a set of our current-voltage data for N-side, C-side, and symmetric dilutions. This model yielded values for the helix dipole effective end-charge (z_0) only slightly below the generally accepted range of ± 0.5 to 0.75 (Hol, 1985) and also, as we found with symmetric 1 M KCl solutions (Kienker et al., 1994a), gave reasonable values for the dielectric constant ratio and image potential width parameters. However, the model could not fit adequately the KCl, pH 7 current-voltage data over the entire range of conditions. The shortcomings of the best-fit model (fit 1 of Table 1) can be seen clearly by examining its predicted reversal potentials (Fig. 10). Although these predictions match the data well for C-side dilutions (corresponding to high cation selectivity), the model predicts equally high anion selectivity for N-side dilutions, rather than the observed lower cation selectivity. The model can fit the reversal potential data somewhat better if these data are fit explicitly (fit 2 of Table 1, Fig. 10); however, the resulting parameters do not fit the currents well (Fig. 11). Allowing the effective partial charges at the N and C termini to assume unequal magnitudes did not improve significantly the fit to the current-voltage data. Finally, the experiment with triethanolammonium glucuronate (Fig. 9) suggests that ionic strength has little effect on charge selectivity in the Ac-(LSSLLSL)$_3$ channel. Hence, the major determinants of charge selectivity could be dipoles that are inaccessible to the bulk electrolyte: for instance, those of the serine hydroxyl groups lining the pore.

Overall, the limitations of this simple electrodiffusion model suggest that a more detailed treatment of the channel charge distribution is needed. Other electrodiffusion models are being developed that can account for more complex phenomena such as sublinear conductance-activity relations (Chen and Eisenberg, 1993; Bek and Jakobsson, 1994).

TABLE 1 Fitted electrodiffusion model parameters

	Fit 1	Fit 2
z_0	0.481	0.364
ϵ_p	9.6	12.9
σ	15.9	17.4
$P_{+/-}$	1.95	5.6
SSE	172	806

Fit 1, best fit to current-voltage data; fit 2, both current-voltage and reversal potential data fit explicitly. z_0 (in units of proton charge), unscreened effective charge at peptide helix N terminus; ϵ_p, dielectric constant of pore lining; σ (Å), characteristic width of dielectric interfacial polarization (image) potential; $P_{+/-}$, intrinsic cation/anion permeability ratio. Both sets of parameters have physically reasonable values, similar to the values obtained from symmetric solution data (Kienker et al., 1994a), although z_0 in fit 2 is somewhat smaller than expected (and, of course, $P_{+/-}$ was not previously evaluated). SSE, sum of squares of the difference between current data and model predictions, provided to indicate the relative goodness-of-fit of all the models.

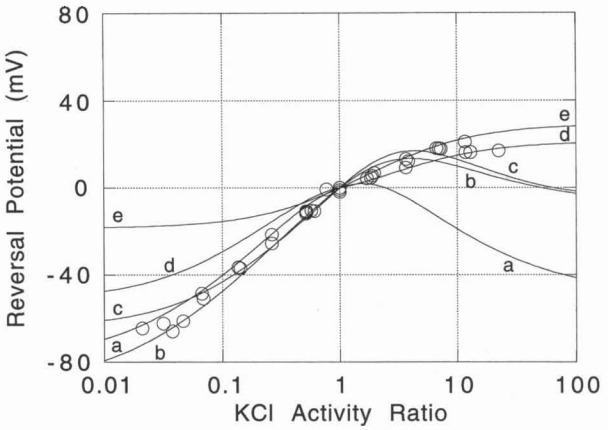

FIGURE 10 Reversal potentials in KCl, pH 7, from Fig. 7, with model fits. Electrodiffusion model (Table 1): (curve a) fit 1; (curve b) fit 2. Site models (Table 2): (curve c) model 4a; (curve d) model 4b; (curve e) C-E-A model.

Cation-anion interaction model

Changes in charge selectivity could also arise from interactions between cations and anions as they pass through the channel. For an uncharged, highly charge-selective channel, it would be reasonable to expect that only one ion at a time could occupy the channel, because ions of like charge repel one another; this assumption leads to fairly tractable permeation models (Hille, 1992). The single-ion occupancy assumption is less compelling in a channel (uncharged or charged) that is permeable to both cations and anions, because opposites attract. For instance, the energy of a lone cation or anion in the channel would be higher than that of a cation-anion pair (although transferring the ion pair from bulk water to an aqueous pore surrounded by a lower dielectric constant membrane environment would still be energetically unfavorable (Parsegian, 1975; Edmonds, 1980)). We have examined some state transition models in which a cation-anion pair can reside in the channel. In the general model, the channel has four states of ion occupancy

$$\begin{array}{ccc} \text{Cation} & \rightleftarrows & \text{Cation} + \text{Anion} \\ \Updownarrow & & \Updownarrow \\ \text{Empty} & \rightleftarrows & \text{Anion}. \end{array} \qquad (3)$$

One could also include direct transitions between the Empty and Cation + Anion states. Model 3 represents only the channel's occupancy states and the transitions among the states. Each arrow represents two ionic transitions; for instance, Empty→Anion is the sum of anion entry rates from both ends of the channel. This model can incorporate asymmetries by assigning different rates to transitions at each end of the channel.

Model 3 can be simplified by eliminating either the cation-occupied state:

$$\text{Empty} \rightleftarrows \text{Anion} \rightleftarrows \text{Cation} + \text{Anion} \qquad (4a)$$

or the anion-occupied state

$$\text{Empty} \rightleftarrows \text{Cation} \rightleftarrows \text{Cation} + \text{Anion}. \qquad (4b)$$

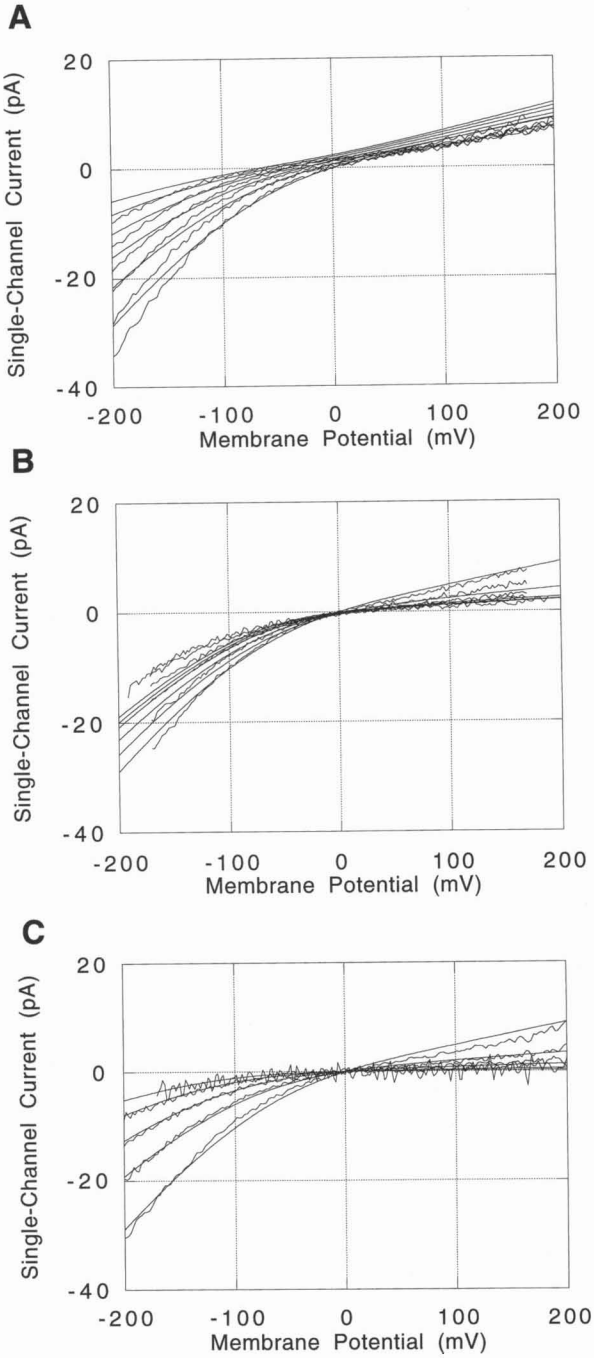

FIGURE 11 Current-voltage data in KCl, pH 7 (*wiggly curves*), as in Figs. 4 and 6, with electrodiffusion model fit 2 of Table 1 (*smooth curves*). [KCl] (M) C-side/N-side, in order of decreasing magnitude of currents at negative potentials, for (*A*) C-side dilutions: 1.0/1.0, 0.49/1.0, 0.24/1.0, 0.12/1.1, 0.053/1.1, 0.024/1.1; (*B*) N-side dilutions: 1.0/1.0, 1.0/0.51, 1.0/0.24, 1.0/0.11, 1.1/0.069, 1.1/0.036. (*C*) symmetric dilutions: as in Fig. 4 legend.

A model similar to model 4a, which requires that an anion occupy the channel before a cation can enter, and that an anion cannot leave while a cation occupies the channel, has been proposed for amphotericin B channels (Borisova et al., 1986). Model 4b, which requires cation occupancy to precede anion entry and anion occupancy to preclude cation exit, is related to a model proposed for hippocampal Cl^- channels

(Franciolini and Nonner, 1987; Franciolini and Petris, 1992), and appears to preserve the interesting features of that model while avoiding the thermodynamic inconsistency of irreversible transitions around a closed reaction cycle without a source of energy.

In the Appendix, we give the predicted current for model 4a as a function of membrane potential, ion activities, and channel characteristics. In this model, anion current results from transitions between the left two states, whereas cation current involves transitions between the right two states. Because the rightward transitions involve a concentration-dependent ion association with the channel, and leftward transitions a concentration-independent ion dissociation, it follows that a high ion concentration tends to drive the reaction scheme to the right, favoring cation current, whereas a low ion concentration favors anion current. Thus, as the ion concentration is lowered, model 4a predicts an increase in anion selectivity. By similar reasoning, model 4b predicts an increase in cation selectivity at lower ion concentration.

We fit model 4a to our KCl, pH 7 current-voltage data (Fig. 12, Table 2). This model fits better than the helix dipole model, but still shows substantial deviations from the current-voltage data. It does fit, however, the reversal potentials about as well as the explicitly fit helix dipole model (Fig. 10). Model 4b fits the current-voltage data better than model 4a, but it does not fit the reversal potentials well for C-side dilutions (Fig. 10, Table 2). A simple single-ion occupancy model does not fit well (Fig. 10, C-E-A fit of Table 2). We cannot make a clear choice between models 4a and 4b; although objectively model 4b fits our current data better, model 4a fits the reversal potentials better. Considering that the qualitative trends in apparent selectivity are important to explain, model 4a and its underlying assumption that anion occupancy is obligatory for cation entry appears to be the slightly preferred choice. At the same time, it can be seen (Fig. 10) from the deviations of the predicted reversal potential curves from the data that none of the models is completely satisfactory in this respect.

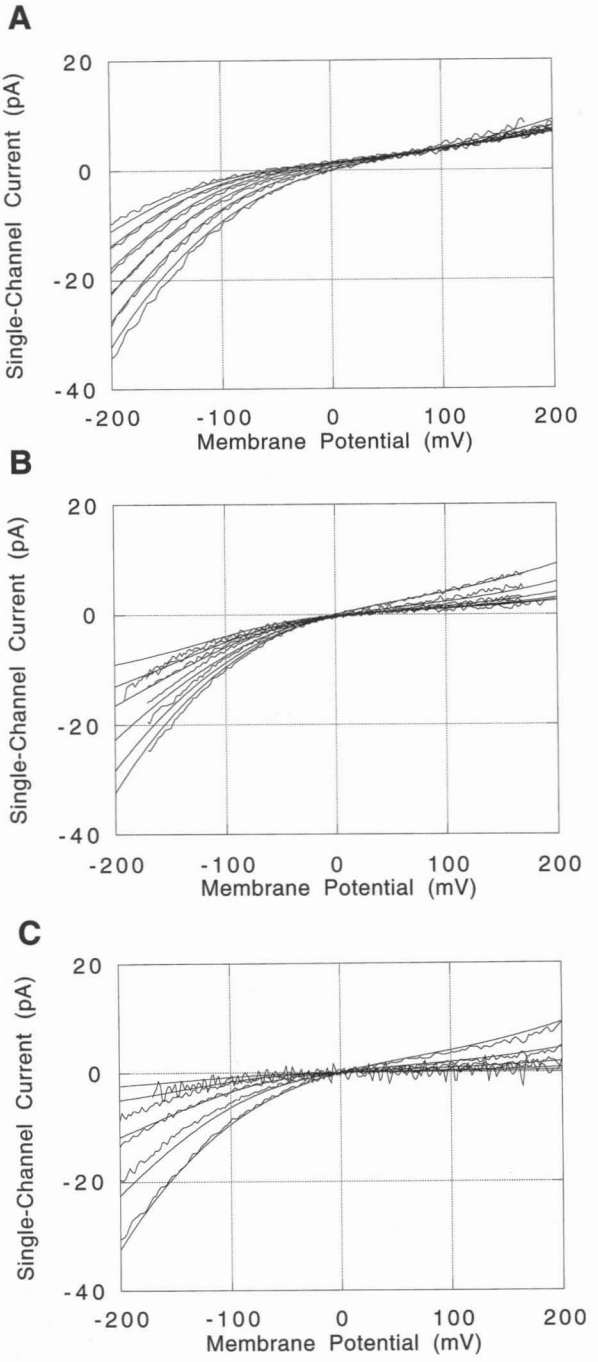

FIGURE 12 Current-voltage data in KCl, pH 7, as in Fig. 11, with fit of model 4a (Table 2).

CONCLUSIONS

Our experience with this particular model peptide system shows that elementary experiments, done on what we believe to be a simple model for a class of biologically relevant ion channel proteins, produce sufficiently complex results to pose a significant challenge to ion channel permeation theory. In our previous study of this system (Kienker et al., 1994a), we fit our current-voltage data in symmetric 1 M KCl to a simple electrodiffusion model using physically reasonable values of our model parameters. That model was extended in the present study, by the addition of a K^+:Cl^- permeability ratio parameter, to fit reversal potential data over a broader range of experimental conditions, with only small changes to the previously fit parameters. However, this extended model cannot fit both the current-voltage data and the reversal potentials satisfactorily with the same set of parameters. The formalism of multi-state ion channel models, containing more parameters, provides a better fit to the current-voltage data with parameters giving reversal potential fits as good as the best electrodiffusion model, but the E-A-CA and E-C-CA models are difficult to distinguish and, accordingly, the parameters of the models are not uniquely interpretable. We hope that application of more rigorous theoretical treatments (Chen et al., 1995) will provide a more accurate, physically interpretable explanation of these data. The remaining experimental challenge will be to use the insights we have gained from these studies to design a "mini-

TABLE 2 Fitted state-transition model parameters

	E-A-CA	E-C-CA	C-E-A
k_{12}^N	6.6*	2.36*	60‡§
k_{21}^N	1.73‡	1.80‡	0.454*
k_{32}^N	3.59‡	3.54‡	60‡§
k_{23}^C/k_{21}^C	100¶§	2.92¶	1.15
k_{21}^C/k_{21}^N	0.085	3.14	5.59
k_{32}^C/k_{32}^N	5.06	9.2	2.11
δ_1^+	0.269	0.146	0.144
δ_2^+	0.250	0.225	0.630
δ_4^+	0.481	0.238	0.226
δ_1^-	0.082	0.474	0.365
δ_2^-	0.107	0.122	0.518
δ_4^-	0.220	0.404	0.117
SSE	122	76	449

Best fits of state transition models to current-voltage data. E-A-CA, model 4a; E-C-CA, model 4b; C-E-A, single-ion occupancy model. The 12 independent parameters that were fit are listed; unlisted parameters can be calculated from this set. The fit parameters are not well constrained. Model 4a parameters are defined in the Appendix. Parameters for the other models are named in an analogous manner, with rate constant subscripts referring to state numbers: E-C-CA, (1) empty, (2) cation, (3) cation + anion; C-E-A, (1) cation, (2) empty, (3), anion. SSE, as in Table 1.

*10^7 s^{-1} mol^{-1}.

‡10^7 s^{-1}.

¶mol^{-1}.

§Parameter was not allowed to exceed this value.

mal" model channel with a level of charge selectivity comparable with that found in the superfamily of ligand-gated ion channels.

Our thanks to Bill DeGrado for providing the peptide and encouragement, to Daniel Camac for technical assistance and lipid purification, to Jim Krywko for molecular modelling help, to Joseph Lazar for mass spectrometry, and to reviewers for their helpful suggestions. Also, thanks to Les Dutton and the Johnson Foundation for their hospitality at the University of Pennsylvania during the completion of this manuscript.

This research was supported in part by the Office of Naval Research.

APPENDIX 1

Cation-anion interaction model

Here we derive a formula for the current for the multi-ion occupancy state transition model 4a, in which a cation can only enter the channel when an anion is bound, and an anion cannot leave the channel while a cation is bound. Closely related models have been applied previously to preferentially anion-selective channels (Borisova et al., 1986; Franciolini and Nonner, 1987), but this model framework can also accommodate channels in which cation conduction predominates. Because of the single-channel current rectification and the asymmetric changes in charge selectivity exhibited by the Ac-(LSSLLSL)$_3$ channel, we do not assume that ion entry or exit rates are the same at the N-side and C-side channel mouths, nor that ion energy barriers are symmetrically located.

In this model, the channel has three states of ion occupancy: (1) empty; (2) anion-bound; (3) both cation- and anion-bound. We allow direct transitions only between states 1 and 2, and between states 2 and 3. We denote the cation and anion activities of the N-side bath by a_+^N and a_-^N, and of the C-side bath by a_+^C and a_-^C, respectively. The membrane potential V is referred to the C-side ground. Parameters used to define the voltage dependence of the rate constants are denoted (starting from the N side) δ_1^s, δ_2^s, δ_3^s, δ_4^s, with $s = +$ or $-$ for the cation or anion energy profile. Defining $B(\delta) = \exp(\delta VF/RT)$ with V the transmembrane voltage, RT/F the constant 25.7 mV (for 298 K), the voltage-dependent rate constants for anion entry into an empty channel from the N and C sides, respectively, are expressed as

$$k_{12}^N B(-\delta_1^-) \tag{A1a}$$

$$k_{12}^C B(\delta_4^-), \tag{A1b}$$

Likewise, anion exit rates to the N and C sides are

$$k_{21}^N B(\delta_2^-) \tag{A2a}$$

$$k_{21}^C B(-\delta_3^-). \tag{A2b}$$

The rate constants for cation entry into an anion-occupied channel are

$$k_{23}^N B(\delta_1^+) \tag{A3a}$$

$$k_{23}^C B(-\delta_4^+), \tag{A3b}$$

and the cation exit rates are

$$k_{32}^N B(-\delta_2^+) \tag{A4a}$$

$$k_{32}^C B(\delta_3^+). \tag{A4b}$$

The δ values can be interpreted as the differences in fractional electrical distances between "wells" and "barriers." With an assumed linear potential drop across the pore, the δ values can be converted to physical distances (L) using the defining relationship:

$$\delta_i = (L_{i-1} - L_i)/L_t$$

where the L values are defined as the distances (measured from the N terminus) of the ith sites or barrier for each ion type. The numbering begins at the N terminus, so $L_0 = 0$ and $L_4 = L_t$. Note that this requires that the δ values for each ion type sum to unity.

For compactness, we define

$$j_{12} = k_{12}^N B(-\delta_1^-)\, a_-^N + k_{12}^C B(\delta_4^-)\, a_-^C \tag{A5a}$$

$$j_{21} = k_{21}^N B(\delta_2^-) + k_{21}^C B(-\delta_3^-) \tag{A5b}$$

$$j_{23} = k_{23}^N B(\delta_1^+)\, a_+^N + k_{23}^C B(-\delta_4^+)\, a_+^C \tag{A5c}$$

$$j_{32} = k_{32}^N B(-\delta_2^+) + k_{32}^C B(\delta_3^+). \tag{A5d}$$

The steady-state probabilities of channel state occupancy are given by $P_i = Z_i/(Z_1 + Z_2 + Z_3)$, $i = 1$–3, with

$$z_1 = j_{32}j_{21} \tag{A6a}$$

$$z_2 = j_{12}j_{32} \tag{A6b}$$

$$z_3 = j_{12}j_{23}. \tag{A6c}$$

The net "C-ward" cation flux at the N-side channel mouth is

$$\Phi_+ = p_2 k_{23}^N B(\delta_1^+)\, a_+^N - p_3 k_{32}^N B(-\delta_2^+), \tag{A7a}$$

and the net anion flux is

$$\Phi_- = p_1 k_{12}^N B(-\delta_1^-)\, a_-^N - p_2 k_{21}^N B(\delta_2^-). \tag{A7b}$$

Then the net current is

$$I = F(\Phi_+ - \Phi_-), \tag{A8}$$

where F is the Faraday constant.

Thermodynamic constraints require

$$k_{12}^C / k_{12}^N = k_{21}^C / k_{21}^N \tag{A9a}$$

$$k_{23}^C / k_{23}^N = k_{32}^C / k_{32}^N. \tag{A9b}$$

Together with the constraints on the fractional electrical distances, this leaves the model with 12 free parameters. The reversal potentials depend only on the ratio of anion exit to cation entry rates, for a total of 7 parameters.

APPENDIX 2

Measures of selectivity

It is widely accepted that ionic selectivity is better reflected by reversal potential measurements than by conductance measurements. This is mainly because the reversal potential is insensitive to block and conductance saturation, according to single-ion occupancy state transition models (Hille, 1992). The reversal potential is most useful when a channel is perfectly selective for one of the ionic species present; equilibrium thermodynamics then requires that the reversal potential equal the Nernst potential for that ion (neglecting osmotic effects). For a channel that is permeable to multiple ionic species, the interpretation of reversal potentials is not so straightforward. The permeability ratio, as calculated from reversal potential data using the Goldman-Hodgkin-Katz theory, is useful as a conventional measure of selectivity for comparing different channels; however, it is not as useful for determining specific selectivity mechanisms, particularly when it is not constant. There are alternative measures of selectivity, such as the cation/anion conductance ratio. This ratio cannot be determined directly from the data; a specific model must be fit to the data, with the conductance ratio then calculated from the fit parameters. Although different selectivity measures generally have different values, our numerical results with model 4a show that the conductance ratio equals the permeability ratio in the equilibrium condition of symmetric bathing solutions and zero voltage, thus defining the "selectivity ratio" $S_{\pm}$

$$S_{\pm} = [(k_{21}^{N})^{-1} + (k_{21}^{C})^{-1}]/[(k_{23}^{N}a_{+}^{N})^{-1} + (k_{23}^{C}a_{+}^{C})^{-1}]. \quad \text{(A10)}$$

Our fit parameters for model 4a give $S_{\pm} = 11$; this is higher than the permeability ratio estimated directly from the pH 7 data, $P_K/P_{Cl} = 5.2$ (Fig. 7), because the model does not fit the data perfectly.

REFERENCES

Adams, D. J., T. M. Dwyer, and B. Hille. 1980. The permeability of endplate channels to monovalent and divalent metal cations. *J. Gen. Physiol.* 75: 493–510.

Åkerfeldt, K. S., P. K. Kienker, J. D. Lear, and W. F. DeGrado. 1995. Structure and conduction mechanisms of minimalist ion channels. *In* Comprehensive Supramolecular Chemistry. D. N. Reinhoudt, editors. Pergamon Press, London. In press.

Åkerfeldt, K. S., J. D. Lear, Z. R. Wasserman, L. A. Chung, and W. F. DeGrado. 1993. Synthetic peptides as models for ion channel proteins. *Acc. Chem. Res.* 26:191–197.

Ammann, D. 1986. Ion-Selective Micro-electrodes. Springer-Verlag, Berlin.

Bek, S., and E. Jakobsson. 1994. Brownian dynamics study of a multiply-occupied cation channel: application to understanding permeation in potassium channels. *Biophys. J.* 66:1028–1038.

Blachly-Dyson, E., S. Peng, M. Colombini, and M. Forte. 1990. Selectivity changes in site-directed mutants of the VDAC ion channel: structural implications. *Science.* 247:1233–1236.

Borisova, M. P., R. A. Brutyan, and L. N. Ermishkin. 1986. Mechanism of anion-cation selectivity of amphotericin B channels. *J. Membr. Biol.* 90: 13–20.

Bormann, J., O. P. Hamill, and B. Sakmann. 1987. Mechanism of anion permeation through channels gated by glycine and γ-aminobutyric acid in mouse cultured spinal neurones. *J. Physiol.* 385:243–286.

Bullock, J. O., E. R. Kolen, and J. L. Shear. 1992. Ion selectivity of colicin E1. II. Permeability to organic cations. *J. Membr. Biol.* 128:1–16.

Chen, D. P., and R. S. Eisenberg. 1993. Flux, coupling, and selectivity in ionic channels of one conformation. *Biophys. J.* 65:727–746.

Chen, D. P., K. Kienker, J. Lear, and R. Eisenberg. 1995. PNP theory fits the current-voltage (IV) relations of a synthetic channel in 7 solutions. *Biophys. J.* In press.

Cohen, B. N., C. Labarca, L. Czyzyk, N. Davidson, and H. A. Lester. 1992a. $Tris^+/Na^+$ permeability ratios of nicotinic acetylcholine receptors are reduced by mutations near the intracellular end of the M2 region. *J. Gen. Physiol.* 99:545–572.

Cohen, B. N., C. Labarca, N. Davidson, and H. A. Lester. 1992b. Mutations in M2 alter the selectivity of the mouse nicotinic acetylcholine receptor for organic and alkali metal cations. *J. Gen. Physiol.* 100:373–400.

Dwyer, T. M., D. J. Adams, and B. Hille. 1980. The permeability of the endplate channel to organic cations in frog muscle. *J. Gen. Physiol.* 75: 469–492.

Edmonds, D. T. 1980. Membrane ion channels and ionic hydration energies. *Proc. R. Soc. Lond. B.* 211:51–62.

Eisenman, G., and R. Horn. 1983. Ionic selectivity revisited: the role of kinetic and equilibrium processes in ion permeation through channels. *J. Membr. Biol.* 76:197–225.

Fatima-Shad, K., and P. H. Barry. 1993. Anion permeation in GABA- and glycine-gated channels of mammalian cultured hippocampal neurons. *Proc. R. Soc. Lond. B.* 253:69–75.

Franciolini, F., and W. Nonner. 1987. Anion and cation permeability of a chloride channel in rat hippocampal neurons. *J. Gen. Physiol.* 90: 453–478.

Franciolini, F., and A. Petris. 1992. Transport mechanisms in chloride channels. *Biochim. Biophys. Acta.* 1113:1–11.

Galzi, J.-L., A. Devillers-Thiéry, N. Hussy, S. Bertrand, J.-P. Changeux, and D. Bertrand. 1992. Mutations in the channel domain of a neuronal nicotinic receptor convert ion selectivity from cationic to anionic. *Nature.* 359:500–505.

Green, W. N., and O. S. Andersen. 1991. Surface charges and ion channel function. *Annu. Rev. Physiol.* 53:341–359.

Grenningloh, G., A. Rienitz, B. Schmitt, C. Methfessel, M. Zensen, K. Beyreuther, E. D. Gundelfinger, and H. Betz. 1987. The strychnine-binding subunit of the glycine receptor shows homology with nicotinic acetylcholine receptors. *Nature.* 328:215–220.

Hall, J. E., I. Vodyanoy, T. M. Balasubramanian, and G. R. Marshall. 1984. Alamethicin. A rich model for channel behavior. *Biophys. J.* 45:233–247.

Hille, B. 1992. Ionic Channels of Excitable Membranes, 2nd ed. Sinauer Associates, Inc., Sunderland, MA.

Hoch, D. H., M. Romero-Mira, B. E. Ehrlich, A. Finkelstein, B. R. DasGupta, and L. L. Simpson. 1985. Channels formed by botulinum, tetanus, and diphtheria toxins in planar lipid bilayers: relevance to translocation of proteins across membranes. *Proc. Natl. Acad. Sci. USA.* 82:1692–1696.

Hol, W. G. J. 1985. The role of the α-helix dipole in protein function and structure. *Prog. Biophys. Mol. Biol.* 45:149–195.

Imoto, K. 1993. Ion channels: molecular basis of ion selectivity. *FEBS Lett.* 325:100–103.

Imoto, K., C. Busch, B. Sakmann, M. Mishina, T. Konno, J. Nakai, H. Bujo, Y. Mori, K. Fukuda, and S. Numa. 1988. Rings of negatively charged amino acids determine the acetylcholine receptor channel conductance. *Nature.* 335:645–648.

Kienker, P. K., W. F. DeGrado, and J. D. Lear. 1993. Rectification and valence selectivity of the uncharged model ion-channel peptide acetyl-(LSSLLSL)$_3$-CONH$_2$. *Biophys. J.* 64:371*a*. (Abstr.)

Kienker, P. K., W. F. DeGrado, and J. D. Lear. 1994a. A helical-dipole model describes the single-channel current rectification of an uncharged peptide ion channel. *Proc. Natl. Acad. Sci. USA.* 91:4859–4863.

Kienker, P., G. Tomaselli, M. Jurman, and G. Yellen. 1994b. Conductance mutations of the nicotinic acetylcholine receptor do not act by a simple electrostatic mechanism. *Biophys. J.* 66:325–334.

Konno, T., C. Busch, E. von Kitzing, K. Imoto, F. Wang, J. Nakai, M. Mishina, S. Numa, and B. Sakmann. 1991. Rings of anionic amino acids as structural determinants of ion selectivity in the acetylcholine receptor channel. *Proc. R. Soc. Lond. B.* 244:69–79.

Langosch, D., K. Hartung, E. Grell, E. Bamberg, and H. Betz. 1991. Ion channel formation by synthetic transmembrane segments of the inhibitory glycine receptor—a model study. *Biochim. Biophys. Acta.* 1063:36–44.

Lear, J. D., Z. R. Wasserman, and W. F. DeGrado. 1988. Synthetic amphiphilic peptide models for protein ion channels. *Science.* 240: 1177–1181.

Lockhart, D. J., and P. S. Kim. 1993. Electrostatic screening of charge and dipole interactions with the helix backbone. *Science.* 260:198–202.

McLaughlin, S. G. A., G. Szabo, G. Eisenman, and S. M. Ciani. 1970. Surface charge and the conductance of phospholipid membranes. *Proc. Natl. Acad. Sci. USA.* 67:1268–1275.

Montal, M., and P. Mueller. 1972. Formation of bimolecular membranes from lipid monolayers and a study of their electrical properties. *Proc. Natl. Acad. Sci. USA.* 69:3561–3566.

Myers, V. B., and D. A. Haydon. 1972. Ion transfer across lipid membranes in the presence of gramicidin A. II. The ion selectivity. *Biochim. Biophys. Acta.* 274:313–322.

Parsegian, V. A. 1975. Ion-membrane interactions as structural forces. *Ann. N. Y. Acad. Sci.* 264:161–174.

Parsons, R. 1959. Handbook of Electrochemical Constants. Butterworths, London.

Raymond, L., S. L. Slatin, and A. Finkelstein. 1985. Channels formed by colicin E1 in planar lipid bilayers are large and exhibit pH-dependent ion selectivity. *J. Membr. Biol.* 84:173–181.

Reddy, G. L., T. Iwamoto, J. M. Tomich, and M. Montal. 1993. Synthetic peptides and four-helix bundle proteins as model systems for the pore-forming structure of channel proteins. II. Transmembrane segment M2 of the brain glycine receptor is a plausible candidate for the pore-lining structure. *J. Biol. Chem.* 268:14608–14615.

Robinson, R. A., and R. H. Stokes. 1968. Electrolyte Solutions. 2nd (revised) ed. Butterworths, London.

Sansom, M. S. P. 1991. The biophysics of peptide models of ion channels. *Prog. Biophys. Mol. Biol.* 55:139–235.

Sather, W. A., J. Yang, and R. W. Tsien. 1994. Structural basis of ion channel permeation and selectivity. *Curr. Opin. Neurobiol.* 4:313–323.

Schofield, P. R., M. G. Darlison, N. Fujita, D. R. Burt, F. A. Stephenson, H. Rodriguez, L. M. Rhee, J. Ramachandran, V. Reale, T. A. Glencorse, P. H. Seeburg, and E. A. Barnard. 1987. Sequence and functional expression of the $GABA_A$ receptor shows a ligand-gated receptor superfamily. *Nature.* 328:221–227.

Unwin, N. 1993. Nicotinic acetylcholine receptor at 9 Å resolution. *J. Mol. Biol.* 229:1101–1124.

Villarroel, A. and B. Sakmann. 1992. Threonine in the selectivity filter of the acetylcholine receptor channel. *Biophys. J.* 62:196–208.

Wada, A. 1976. The α-helix as an electric macro-dipole. *Adv. Biophys.* 9:1–63.

Wang, F., and K. Imoto. 1992. Pore size and negative charge as structural determinants of permeability in the *Torpedo* nicotinic acetylcholine receptor channel. *Proc. R. Soc. Lond. B.* 250:11–17.